856 *Macromolecules* **2010**, *43*, 856–867
DOI: 10.1021/ma902213p

Macromolecules
ARTICLE

Synthesis of Polymer/Silica Hybrid Nanoparticles Using Anionic Polymerization Techniques

Eike Hübner, Jürgen Allgaier,* Mathias Meyer, Jörg Stellbrink, Wim Pyckhout-Hintzen, and Dieter Richter

Institut für Festkörperforschung, Forschungszentrum Jülich GmbH, 52425 Jülich, Germany

Received October 6, 2009; Revised Manuscript Received November 26, 2009

ABSTRACT: We report a new "grafting to" technique for the functionalization of silica particles with anionically produced polymers. It is based on a two-step procedure. In the first step the silica nanoparticles were modified with multifunctional chlorosilanes. This procedure allows replacing the original Si−OH surface groups by Si−Cl groups. In the second step the anionically synthesized polymers were linked to the Si−Cl functionalized nanoparticle surface. Both the chlorosilane functionalization of the nanoparticles and the subsequent reaction with living polymer can be carried out without irreversible particle aggregation. This was proved by examining the reaction products with static and dynamic light scattering as well as small-angle X-ray scattering. The polymer linking event is accompanied by termination reactions, most likely due to residual Si−OH groups. Therefore, the raw products were purified by a simple fractionation procedure. The examination of the products by size exclusion chromatography showed that this procedure allowed removing the free polymer quantitatively. The new anionic based method offers the possibility for grafting densities up to 1 chain per nm^2 of particle surface, which is significantly higher than reported in the past for other "grafting to" approaches. The now obtained grafting densities are similar to the ones reported for "grafting from" techniques which are mainly based on controlled radical polymerization. Our new approach offers the possibility to obtain hybrid materials containing polymers which are not accessible via controlled radical techniques like polydienes. In addition, the new technique allows grafting polymers having molecular weights up to 500 000 g/mol and still narrow molecular weight distributions.

Introduction

Core−shell hybrid nanoparticles usually consist of an inner solid and inorganic core surrounded by a soft polymer shell. Typical examples for the inner part are SiO_2, Fe_2O_3, and other transition metal oxides or small metal clusters such as Au or Si particles, while the shell is based on polymers such as polystyrene or polyacrylates.[1] Frequently, the interest of such materials is focused on the properties of the core material, in terms of optical or magnetic properties,[1,2] whereas the polymer shell acts as a compatibilizer to render the inorganic substrate soluble or dispersible in a matrix polymer and prevents particle aggregation. On the other hand, the polymer shell can carry various functional groups for further interactions such as highly charged polymer chains.[1,3] Furthermore, a combination of the core and shell characteristics can lead to distinctive optical and mechanical properties.[4] Interactions of the polymer shell with the matrix become more important with increasing shell thickness, corresponding to a higher molecular weight of the grafted polymer.

The most precise way to obtain hybrid nanoparticles is the covalent fixation of the polymer at the nanoparticle surface by reactive end groups. In general, two synthetic pathways are possible: "grafting from" and "grafting to".[1] The "grafting from" approach starts with the covalent attachment of a polymerization initiator onto the particle surface and subsequent addition of monomers. Controlled radical polymerization techniques have been applied very successfully in the synthesis of such particles, mainly "atom transfer radical polymerization" (ATRP) and "reverse addition−fragmentation chain transfer" (RAFT) mediated polymerization.[1,2,5−9] However, limitations occur due to the radical polymerization process. Radical recombination can lead to cross-linking on the surface of the same particle or interparticle linking.[10,11] The latter process is of special relevance with increasing number of chains per particle. Furthermore, after finished polymerization, the chain ends are still reactive. This leads to particle cross-linking at higher temperatures due to uncontrolled radical reactions. Various deactivation methods are known in the literature,[12,13] but care has to be taken to quantitatively deactivate all chain ends since just a small fraction of still active chain ends can cause complete cross-linking of the hybrid particles.

In addition, termination processes of the growing polymer chains limit the accessible molecular weight of the attached chains using controlled radical techniques.[14] Especially for styrene, molecular weights above 40 000 g mol^{-1} lead to molecular weight distributions above 1.1. Recent enhancements of ATRP, such as ARGET (activators regenerated by electron transfer) ATRP, allow achieving relatively low molecular weight distributions in the molecular weight range of 100 000−200 000 g mol^{-1}. However, an increased amount of radical recombination makes it difficult to use this techniques for "grafting from" small particles due to interparticle cross-linking.[15]

The usage of anionic polymerization together with the "grafting from" approach allows reaching high molecular weights and narrow polydispersities. But, because of reactive surface groups and adsorbed impurities, living anionic polymerization is barely usable for "grafting from" particles and mainly restricted to clean, macroscopic surfaces such as gold.[5,16]

The second synthetic pathway to core−shell hybrid nanoparticles uses the "grafting to" approach. In this technique, the

*Corresponding author: e-mail j.allgaier@fz-juelich.de; Tel +49 2461 61 2541; Fax +49 2461 61 2610.

 Published on Web 12/16/2009

polymer is synthesized first. After functionalization, the chain ends are covalently attached to the particle surface. Examples in the literature include the grafting of anionically polymerized styrene or of polyethylene obtained from metallocene-catalyzed polymerization on silica surfaces. In both cases the chain ends were functionalized with chlorosilane linking groups.[17−20] However, because of the slow reaction of the linking groups with the Si−OH functionalities of the particle surface the measured grafting densities were low. They range from 0.35 chains/nm^2 for polystyrene having a molecular weight of 4700 g mol^{-1} and decrease to 0.16 chains/nm^2 at a molecular weight of 24 000 g mol^{-1}. For polyethylene with a molecular weight of 325 000 g mol^{-1} only 0.001 chains/nm^2 were found.[17,18] These grafting densities are much below the grafting densities accessible by "grafting from" approaches which are in the range of 1 chain/nm^2 and do not decrease with increasing molecular weight.[7]

In this work, we report a new "grafting to" technique for the functionalization of silica particles using anionic polymerization. It is based on a two-step procedure. In the first step the silica particles were modified with chlorosilanes having at least two Si−Cl functionalities. This procedure allowed replacing the original Si−OH surface groups by Si−Cl groups. The details of the chlorosilane functionalization were studied with different multifunctional chlorosilanes. In the second step anionically synthesized polymers were linked to the nanoparticles. The reaction of the polymeric carbon−lithium headgroups with the chlorosilane surface groups was studied as a function of the polymer molecular weight and the nature of the headgroup. In addition, the influence of the chlorosilane surface density and the concentration of living polymer on the achievable polymer grafting density were tested.

Experimental Section

Experimental Equipment. All operations with air-sensitive compounds were carried out at a high-vacuum line using Schlenk techniques or in a glovebox (M Braun, Unilab) under argon. The water level and the oxygen level in the glovebox were below 1 and 0.1 ppm, respectively. The Schlenk flasks were equipped with Teflon stopcocks that allowed transferring materials between the vacuum line and the glovebox without contamination with air. The flasks that were exposed to overpressure during the polymerization of butadiene were pressure-tested to 4−12 bar depending on the size of the flask. A Sigma 4K15C laboratory centrifuge was used for centrifugation. IR spectra were recorded by use of a Shimadzu IR-470 IR spectrometer in CaF_2 cuvettes (0.2 mm).

Materials. Benzene (Merck, ≥99.7%) and cyclohexane (Merck, ≥99.5%) were degassed and distilled over *n*-butyllithium before use. Tetrahydrofuran (THF) (Merck, 99.9%) was degassed, predried over CaH_2, and dried with Na/K and benzophenone before use. Styrene (Fluka, ≥99%) was degassed and stirred over di-*n*-butylmagnesium overnight at 0 °C and distilled directly into the reactor before use. Butadiene (Aldrich, 99+%) was condensed on di-*n*-butylmagnesium, stirred at 0 °C overnight, condensed on *n*-butyllithium, stirred below −20 °C for 20 min, and directly before use it was condensed into the polymerization flask. Dimethyldichlorosilane (Me_2SiCl_2) (Aldrich, >99.5%), trimethylchlorosilane (Me_3SiCl) (Aldrich, 99+%), and tetrachlorosilane ($SiCl_4$) (Aldrich, 99%) were distilled at the vacuum line. The first fraction was discarded and only the middle fraction was used, which contained about 1/3 of the original material. Toluene (Merck, ≥99.9%), methanol (Merck, ≥99.9%), *n*-butyllithium (Aldrich, 1.6 M in hexane), *sec*-butyllithium (Aldrich, 1.4 M in cyclohexane), *tert*-butyllithium (Aldrich, 1.7 M in pentane), di-*n*-butylmagnesium (Aldrich, 1.0 M in heptane), 2,6-di-*tert*-butyl-4-methylphenol (BHT) (Aldrich, 99%), and 2-cyanoethylmethyldichlorosilane (ABCR, 97%) were used as received. The polymerization initiators *tert*-butyllithium and *sec*-butyllithium were diluted in dry benzene or cyclohexane, respectively, and the exact concentration was determined by Gilman double titration.[21] Silica nanoparticles (R = 10 nm) were obtained as 30 wt % solution in *n*-butyl acetate from Nissan (NBAC-ST) and used as received.

Chlorosilane Functionalization of Nanoparticles. In a 100 mL flask 8.0 g of 30 wt % NBAC-ST solution was degassed five times under continuous stirring at room temperature for 2 h. The evacuated flask was transferred into the glovebox, and 30 mmol of the appropriate chlorosilane was added using a balance installed in the glovebox. The solution turned slightly turbid and was stirred for 72 h. Excess chlorosilane, *n*-butyl acetate, and HCl formed during the reaction were condensed into a small flask and disposed in ice/water. The white, powdery residue was dried for 48 h at high vacuum during slow stirring of the dry powder and stored inside the glovebox. The functionalized particles were redisperged in dry toluene and used without purification for analysis by dynamic light scattering and further functionalization. Samples of the particles were sealed in glass tubes under argon for the transport to analytical laboratories for the chlorine content determination.

Polymerization Reactions. All polymerization reactions were carried out in Schlenk glass flasks equipped with Teflon stopcocks. The flasks were evacuated and heated before use. The flasks were charged with a solution of *tert*-butyllithium for the polymerization of butadiene and *sec*-butyllithium for the polymerization of styrene. After pumping off the argon at the vacuum line, the monomer and benzene were condensed onto the frozen initiator solution. The weight ratio of monomer to solvent was around 1:10. The polymerization flasks were allowed to warm up and stirred for 2 days in a water bath at room temperature. Then samples were taken inside the glovebox with a dry syringe, terminated with degassed methanol, and precipitated in methanol. In the case of polybutadiene, a small amount of BHT was added to the methanol as stabilizing agent. In case of end-capping of living polystyrene with butadiene the solution was cooled to 0 °C, and the appropriate amount of dry butadiene was condensed into the solution so that the polystyryllithium headgroups were capped on average with four butadiene units.

Linking of the Polymer onto the Chlorosilane-Functionalized Nanoparticles. The chlorosilane-functionalized nanoparticles were filled in a dry Schlenk flask and dissolved with dry benzene inside the glovebox. The concentration of the solution was 10 wt %. After 18 h, the solution of the living anionic polymer in benzene was added with a dry syringe. The mole ratio of Si−Cl to living anionic polymer was varied between 0.5 and 3. The solution was stirred, and samples were taken during a period of 3 weeks to monitor the progress of the reaction by size exclusion chromatography (SEC). After the SEC analysis indicated no further reaction, a small amount of methanol was added. The reaction product was precipitated in methanol. In the case of polybutadiene, a small amount of BHT was added to the methanol as stabilizing agent.

Fractionation. To separate free polymer from the functionalized nanoparticles, the crude mixture was dissolved in toluene. The total concentration was 0.4 wt %. Methanol was slowly added until the mixture turned suddenly turbid. The suspension was slowly warmed up, and the addition of methanol was continued to keep the mixture slightly turbid. At 36−37 °C the addition of methanol was stopped and slowly heated until the mixture turned completely clear. Typically, an amount of 20 vol % methanol was necessary to reach the desired temperature. Then the solution was allowed to cool down overnight in a separating funnel. In case of a molecular weight of the grafted polymer of about 10 000 g mol^{-1}, the resulting strongly turbid suspension was centrifuged. The clear supernatant solution was removed, and the residue was dried in high vacuum and analyzed by SEC to ensure absence of free polymer. In case of a molecular weight of the grafted polymer of about 100 000 g mol^{-1},

the functionalized particles precipitate as large flocks at the bottom of the separating funnel. The flocks were transferred together with small parts of clear solution into centrifuge vessels and centrifuged. The clear supernatant solution was removed, and the residue dried in high-vacuum and analyzed by SEC to ensure absence of free polymer. In case of a molecular weight of the grafted polymer of about 500 000 g mol^{-1}, the concentration of the solution for the fractionation process was lowered to 0.1 wt % and addition of methanol was stopped at 26−27 °C. The further work-up was analogous to the fractionation of particles with a molecular weight of the grafted polymer of about 100 000 g mol^{-1}. In some cases the fractionation process was repeated to remove small residues of free polymer still being present in the product.

Characterization. The SEC experiments were carried out using a PL-GPC 50 instrument for the analysis of the pure polymer samples. Three Polypore (Polymer Laboratories) 5 μm columns (molecular weight operating range 200−2 000 000 g/mol) at 30 °C were used. For the signal detection a Viscotek model TDA 300 detector with differential refractometer (RI) detector at 650 nm and a 90° laser light scattering (LS) detector at 670 nm was used at 30 °C. The solvent was THF at a flow rate of 1 mL/min, which was degassed with a Viscotec model VE 7510 instrument. Molecular weights were calculated from the results of the LS and RI detector using the Polymer Laboratories Cirrus GPC software. Molecular weight distributions were obtained using conventional polystyrene calibration. For the high molecular weight polymer **PB4** four PLgel 10 μm MIXED-B columns (linear range of molecular weight 500−10 000 000 g/mol) were used to analyze the molecular weight distribution. The molecular weight of **PB4** was determined with a Dawn Heleos-II multiangle light scattering instrument from Wyatt Technology at a wavelength of 658.0 nm with five concentrations in *n*-heptane at room temperature. All solutions were filtrated before use. Molecular weight, R_g, and A_2 were calculated from a standard Berry plot with the software provided with the instrument. The dn/dc value was measured at five concentrations at a wavelength of 658.0 nm with a Optilab rEX refractive index detector from Wyatt Technology. For the analysis of samples containing functionalized particles a PL-GPC 220 instrument with three Polypore (Polymer Laboratories) 5 μm columns at 30 °C and RI detector at 890 nm was used. The solvent was a mixture of THF and *N,N*-dimethylacetamide (DMA) (85:15% (v:v)) at a flow rate of 1 mL/min.

Dynamic light scattering (DLS) experiments were performed on an ALV SP-125 (ALV, Germany) compact goniometer using an argon ion laser (Coherent, Innova 90-4) operating with vertically polarized light at $\lambda_0 = 514.5$ nm and $I_0 = 50-100$ mW. Intensity autocorrelation functions were recorded with an ALV 5000 E (fast version, 319 channels) multitau digital correlator. The hydrodynamic radii R_h presented here were obtained from a inverse Laplace transformation using the regularized CONTIN algorithm with 150 grid points with the ALV-5000/E software version 1.4.8.2 from measurements at 90° scattering angle. Diffusion coefficients have been transformed to R_h assuming a logarithmic mass-weighting as implemented in the software. The measurements of the chlorosilane-functionalized nanoparticles were carried out in cuvettes, equipped with Teflon stopcocks. The cuvettes were filled in a glovebox. Dry toluene was used as solvent. Static light scattering data were corrected for background scattering and normalized by the Rayleigh ratio of toluene and analyzed using standard Zimm plots. Small-angle X-ray scattering (SAXS) studies were performed using a NANOSTAR-U camera (Bruker AXS). The instrument was equipped with a rotating anode source, run at 40 kV and 40 mA, and filtered to yield only Cu Kα with wavelength $\lambda = 1.540$ Å. The collimation path consisted of three pinholes, and the primary beamstop was 2 mm in diameter. Two-dimensionally obtained scattering patterns were collected on a Hi-Star xenon-filled 1000 × 1000 wired grid area detector. Transmissions were obtained from absorbance measurements using a glassy carbon standard which was inserted in the optical path between sample and detector. The spot size of the beam on the sample was 500 μm. All data were corrected for detector sensitivity, background scattering, and dark current noise after radially averaging to yield a usable scattering vector range about $0.01 < q < 0.20$ $Å^{-1}$. Some excess intensity at low q may remain, which is typical for catalyst residues, bubbles, and voids or even due to the subtraction of not identically scattering empty capillaries.

Elemental analysis of the chlorine content were performed by the "Mikroanalytisches Labor Pascher" in D-53424 Remagen, Germany, and samples were handled under inert gas conditions. Elemental analysis of the carbon, hydrogen, nitrogen, and oxygen content were performed by the analytical laboratories of the Forschungszentrum Jülich. The carbon content was measured with a LECO system using an IR detector after burning the sample at 2300 °C in an oxygen atmosphere. The oxygen content was measured by heat extraction in a helium atmosphere and IR detection. Nitrogen and hydrogen content were measured with a LECO system CHNS analyzer.

Results

The synthesis of star polymers from living anionic polymers such as polystyryllithium, polyisoprenyllithium, or polybutadienyllithium and chlorosilane linking reagents is a well-known reaction.[22−27] Star polymers with up to 64 arms and narrow distributions with respect to arm numbers were synthesized with the help of dendritic chlorosilanes.[27] Because of the high reactivity of the anionic headgroups, the functionalization of nearly all Si−Cl linking groups of the dendritic chlorosilane was possible.[27] The structure of such multiarmed star polymers can be considered to be comparable to a core−shell particle. A similar strategy we applied now for the synthesis of polymer/silica hybrid nanoparticles. It is outlined in Scheme 1.

Silica was chosen as core material, since spherical silica particles are accessible from nanometer to micrometer scale in rather low polydispersities and the silica surface contains Si−OH groups which can be easily functionalized.[28] To ensure functionalization of single nanoparticles without agglomeration, hydrophobically modified particles dispersed in *n*-butyl acetate (NBAC-ST) were selected. Previous results from Matyjaszewski and Oberdisse have proven the absence of particle aggregation during the reaction of comparable particles in organic solvents with other silane compounds.[7,8] In addition, *n*-butyl acetate is inert against the functionalization reagents and possible side-products formed during the functionalization. Generally, a silica surface contains about 5−6 Si−OH groups per nm^2. In the case of the silica used in this work about 20% of them are modified with alkylsilane groups (mainly O−$SiMe_3$) in order to stabilize the particle in the organic solvent. If this is taken into account, about 4.4 Si−OH groups per nm^2 still exist on the particle surface. The mean radius of the particles according to the supplier is about 10 nm, and its density is 2.0 g cm^{-3}. On this basis each nanoparticle contains 5500 surface Si−OH. These values are used later for further calculations.

Functionalization of the Nanoparticles with Chlorosilanes. The reaction of macroscopic silica surfaces with chlorosilanes has been intensively studied.[29−31] For nonaggregated silica nanoparticles only monofunctional chlorosilanes were used so far. In this work, we expanded the use to multifunctional chlorosilanes using Me_2SiCl_2, a mixture of Me_2SiCl_2 and Me_3SiCl in the molar ratio of 1:3, $SiCl_4$, and $SiMe(CH_2CH_2CN)Cl_2$ (Scheme 2). In all cases, the molar ratio of chlorosilane compared to the calculated amount of surface Si−OH was 10:1. The synthesis details are given in the Experimental Section. After removal of all volatile

Scheme 1. Concept for the Synthesis of Polymer/Silica Hybrid Nanoparticles Using Me_2SiCl_2 as Chlorosilane Compound

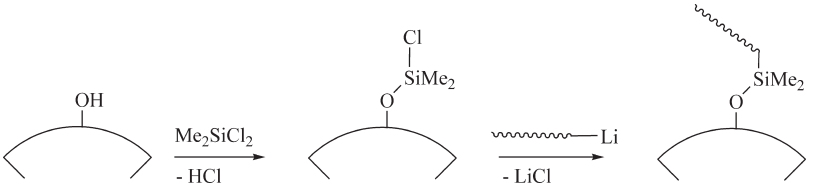

Scheme 2. Functionalization of Silica Particles with Me_2SiCl_2, Me_3SiCl, $SiCl_4$, and $SiMe(CH_2CH_2CN)Cl_2$

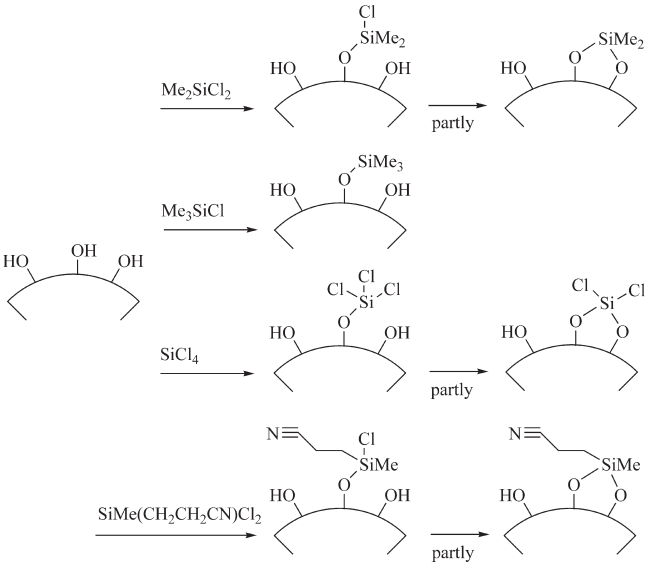

Table 1. Characterization of the Si−Cl Functionalized Nanoparticles

particle	functionalization agent	Cl content (mmol g^{-1})	Si−Cl/ nm^2	N content (mmol g^{-1})	R_h (nm)
unmodified particles				< 0.01	15
SiO_2-Cl-I	$SiMe_2Cl_2$	0.28	1.12		13
SiO_2-Cl-II	$SiMe_2Cl_2$/$SiMe_3Cl$ (1:3)	0.09	0.36		*a*
SiO_2-Cl-III	$SiCl_4$	1.26	5.06		15[b]
SiO_2-Cl-IV	$SiMe(CH_2CH_2CN)Cl$	0.57	2.28	0.94	

[a] Not redispersible. [b] Contains unsoluble residues.

material, the chlorine contents were measured by elemental analysis. The results are summarized in Table 1.

The functionalized nanoparticles obtained after reaction with $SiMe_2Cl_2$, **SiO_2-Cl-I**, were found to be redispersible in nonpolar solvents such as dry benzene and toluene. In the case of nonfunctionalized particles drying leads to irreversible aggregation. This difference can be explained by the additional stabilization via the chlorosilane. The amount of chlorine was determined by elemental analysis. For **SiO_2-Cl-I** a value of 0.28 mmol g^{-1} was found. Assuming the above given details for the particle size and density, this leads to 1.12 linking sites per nm^2 or in other words 1400 Si−Cl groups per particle. This functionality is in the range typically reported for the functionalization of silica particles with other monofunctional chlorosilane reagents.[7] The absence of particle aggregation upon reaction with $SiMe_2Cl_2$ was not necessarily expected since the difunctional chlorosilane could connect different particles. Because of the large number of Si−Cl groups per particle, already a small fraction of bridging reactions would lead to strong interparticle crosslinking. The use of an excess of chlorosilane suppresses this process. In addition, the reactivity of the second Si−Cl group to undergo a bridging reaction is expected to be drastically reduced for sterical reasons.

To lower the amount of reactive Si−Cl groups, a mixture of Me_2SiCl_2 and Me_3SiCl was applied in the functionalization of the particles. Simple reduction of the Me_2SiCl_2 amount could not be applied as this measure would provoke particle aggregation. Moreover, the O−$SiMe_3$ groups resulting from the reaction with Me_3SiCl are unreactive toward living anionic polymers (Scheme 2) whereas residual Si−OH groups would terminate them. A mixture of Me_2SiCl_2 and Me_3SiCl in the ratio 1:3.1 consequently led to a lower amount of chlorine in sample **SiO_2-Cl-II**. Assuming an identical degree of functionalization as for **SiO_2-Cl-I**, the chlorine content found of 0.09 mmol g^{-1} is slightly higher than expected from the molar ratio of the silane compounds (0.07 mmol g^{-1}). This can be explained by a higher reaction rate of dichlorodimethylsilane with Si−OH compared to trimethylchlorosilane.[30] However, the functionalized particles could not be redispersed in toluene or benzene.

In order to achieve a higher degree of Si−Cl functionalization, the silica nanoparticles were functionalized with $SiCl_4$ (Scheme 2). The elemental analysis of the corresponding sample **SiO_2-Cl-III** revealed a functionalization degree of 1.26 mmol Cl g^{-1}, which translates into 5.06 Si−Cl bonds per nm^2. Under the assumption that only one Si−Cl group per chlorosilane molecule reacts with the silica surface, the results for sample **SiO_2-Cl-III** are distinctly higher than expected from the results for sample **SiO_2-Cl-I**. However, it is obvious that more than one Si−Cl group of a chlorosilane molecule can react with the silica surface (Scheme 2).[31] Under this assumption the amount of reacted chlorosilane is higher than indicated by the Si−Cl functionalization.

In order to obtain a deeper understanding of the linking reaction, the silica nanoparticles were functionalized with $SiMe(CH_2CH_2CN)Cl_2$. This compound may form one or two bonds with the silica surface but allows to distinguish between the two species by comparing the nitrogen and the chlorine content of the functionalized silica particles. The nitrogen content was found to be remarkably higher than the chlorine content (sample **SiO_2-Cl-IV**). From the values given in Table 1 the fractions of single and double bound chlorosilane could be calculated to be 61% and 39%, respectively. The higher overall functionalization degree of **SiO_2-Cl-IV** may be explained by the polarity of the cyano group and therefore good accessibility of the Si−OH surface. Assuming the same ratio of single to double bound species for the reaction with Me_2SiCl_2, sample **SiO_2-Cl-I** contains 1.12 Si−Cl groups and 0.72 $SiMe_2$ groups per nm^2; this corresponds to 2.56 reacted Si−OH groups per nm^2. If the hydrophobical modification of the nanoparticles by the supplier is taken into account, about 67% of the original Si−OH groups have reacted. If the same scenario is applied for the functionalization with $SiCl_4$ and the identical surface densities of single and double bound chlorosilane are assumed as before, one would expect 1.2 mmol Cl g^{-1}, corresponding to 4.80 Si−Cl units per nm^2. This value matches nicely with the elemental analysis result of **SiO_2-Cl-III** of 1.26 mmol g^{-1} given in Table 1.

Further experiments with Me_2SiCl_2 by increasing the reaction time and the reaction temperature did not reduce the amount of residual Si−OH. In case of functionalization reactions with initiators for controlled radical polymerizations, the use of monofunctional chlorosilanes was reported. In our case, however, the Si−Cl functionality must be at least two. This could cause particle−particle coupling. Samples **SiO_2-Cl-I** and **SiO_2-Cl-III** could be solubilized easily after having removed excess chlorosilane. This excludes at least large scale interparticle linking. To check whether the fuctionalization lead to minor interparticle linking, samples **SiO_2-Cl-I** and **SiO_2-Cl-III** were examined by DLS. The measurements were carried out under inert gas atmosphere to prevent subsequent cross-linking by moisture.

DLS measurements showed a hydrodynamic radius of $R_h = 15$ nm for the unmodified nanoparticles. Similar small silica particles in water have recently been investigated in detail and were characterized to be based on a compact inner core and thin softer shell, which may explain the different results for the radius obtained with different analytical methods.[28,32] No indication for aggregation or interparticle linking was found in case of **SiO_2-Cl-I** redispersed in toluene; R_h was identical to the unmodified particles within the experimental error (see Table 1). The increase in size due to the functionalization can be neglected. The calculated mass increase resulting from this reaction is about 5%, and the corresponding theoretical increase in radius is less than 2%.

Table 2. Characterization of the Polymers Used for Nanoparticle Functionalization

polymer	initiator	M_n[a] (g/mol)	M_w/M_n[b]	R_g[c] (nm)	R_h[d] (nm)
PB1	*t*-BuLi	15 300	1.01	4.5	3.6
PB2	*t*-BuLi	105 000	1.03	14.7	10.9
PB3	*t*-BuLi	13 000	1.01	4.1	3.3
PB4	*t*-BuLi	589 000[e]	1.04	42.1	29.2
PS1	*s*-BuLi	10 100	1.03	2.9	2.1
PS-PB1	*s*-BuLi	9 900	1.02		

[a] From SEC with LS detection. [b] From SEC with PS calibration. [c] Radii of gyration in cyclohexane, calculated from ref 33. [d] Hydrodynamic radii in cyclohexane, calculated from ref 33. [e] From off-line LS in heptane.

The result not only proves the absence of interparticle linking during the functionalization with the chlorosilane but also shows that the solvent exchange does not cause irreversible particle aggregation. The functionalization with a mixture of Me_2SiCl_2 and Me_3SiCl lead to insoluble particles in sample **SiO_2-Cl-II**. In the case of sample **SiO_2-Cl-III** insoluble residues were noticed after redispersion in toluene. After centrifugation in a sealed flask the hydrodynamic radius of the soluble particles fraction was found to be unchanged at $R_h = 15$ nm. The nature of the insoluble residues will be discussed in the context of the reactions with living polymer in the next paragraph.

Functionalization of the Chlorosilane-Modified Nanoparticles with Living Anionic Polymers. The next step in the synthesis of the hybrid nanoparticles is the linking of the living anionic polymer onto the functionalized particles. The characterization of the polymers used in this work is summarized in Table 2.

First, 1,4-polybutadiene was chosen since it is not accessible via controlled radical polymerization techniques. Because of the small size of the butadienyllithium headgroup, the sterical hindrance for the reaction with the Si−Cl group is reduced to a minimum. The linking reaction is shown in the upper part of Scheme 3. Benzene was used for the polymerization since the anionic headgroups are stable in this solvent and the functionalized nanoparticles can be dispersed. In a first experiment, the living polymer **PB1-Li**, having a molecular weight of 15 300 g/mol, was mixed with the $-SiMe_2Cl$ functionalized nanoparticles **SiO_2-Cl-I**, which were dispersed before in benzene. The molar ratio of Si−Cl to **PB1-Li** was 1:1.5. Upon mixing, the solution was clear. It turned slightly turbid and became clear again after some hours.

The linking reaction was monitored by SEC. The lower trace in Figure 1 shows the SEC chromatogram of the raw product **SiO_2-I-PB1**. The upper trace corresponds to the precursor **PB1** taken before the linking reaction. In the lower chromatogram the right signal at 21.9 min corresponds to free polymer. The small signal to the left at 20.8 min shows twice the molecular weight, and furthermore extremely small amounts of even higher molecular weights can be noticed.

Scheme 3. Linking Reactions of Living Anionic Polymers onto Si−Cl Functionalized Silica Nanoparticles

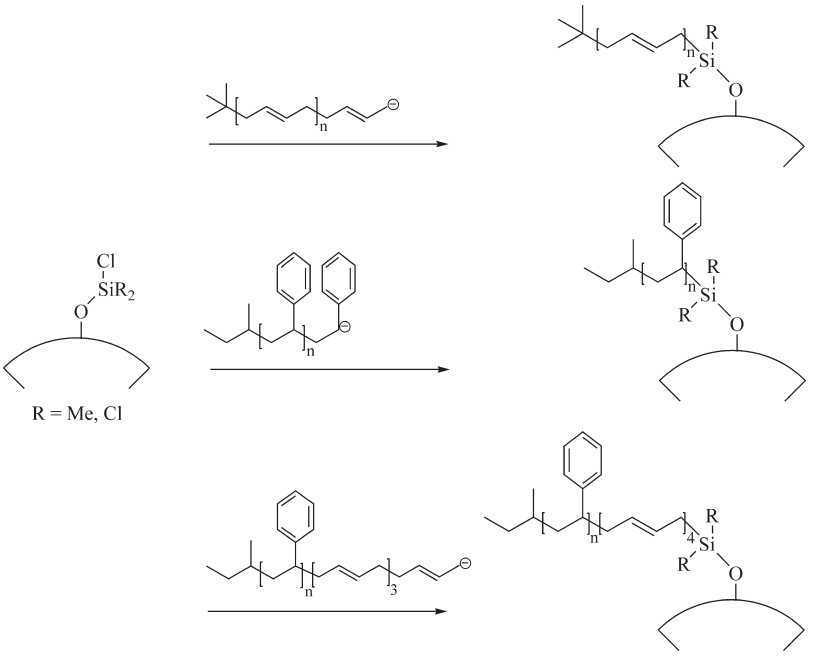

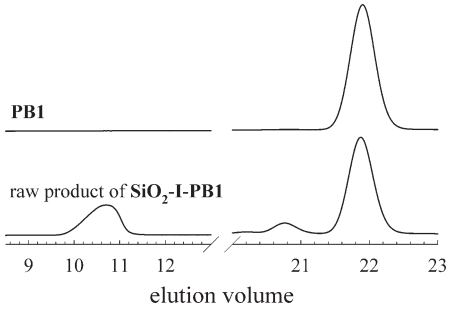

Figure 1. SEC chromatograms of the polybutadiene precursor **PB1** (upper trace) and the raw product of the linking reaction with the functionalized nanoparticles **SiO_2-Cl-I** (lower trace).

It is unlikely that residues of Me_2SiCl_2 caused this coupled product due to the drying process of **SiO_2-Cl-I** under high-vacuum conditions for several days. A coupling reaction caused by oxygen contamination via a leak in the reactor is unlikely, too, as the intensity ratio of the signals between 20.8 and 21.9 min stayed constant over weeks.

The peak at an elution time between 10 and 11 min is assigned to the functionalized nanoparticles. The signal occurs at an elution time above the upper exclusion limit of the SEC columns. Both the elution time and the signal shape varied from experiment to experiment. Therefore, the high molecular weight signal contains no reliable information with respect to molecular weight or distribution of the functionalized nanoparticles. The use of special SEC columns for high molecular weight polymers lead to the same result. Therefore, it has to be assumed that the size of the functionalized hybrid nanoparticles is too large for conventional SEC characterization. Nevertheless, SEC is a convenient tool to follow and quantify the linking reaction as RI signal intensity is directly proportional to concentration. Therefore, the comparison of the precursor **PB1** and raw product samples of known concentration allows to detect the amount of nonlinked polymer. This procedure could not be applied to the signal of the hybrid nanoparticles, possibly because of incomplete or partially retarded elution.

From the SEC signal intensity of the free polymer in sample **SiO_2-I-PB1** after 2 weeks, the linking degree was calculated to be 43% of the original **PB1-Li**. No further increase was noticeable after longer reaction times. Because of the 1.5-fold excess of living polymer over Si−Cl groups, 65% of the chlorosilane groups were functionalized with a polymer chain. In order to test the livingness of the so far unreacted polybutadiene, new butadiene was condensed onto the reaction mixture. The SEC chromatogram of an isolated sample taken 2 days later showed no elution time increase of the free polymer. Therefore, it has to be assumed that all polymer was terminated due to side reactions such as protonation with residual Si−OH groups of the nanoparticle surface.

To check the stability of the living anionic polybutadiene, a sample of the poly(butadienyllithium) in benzene was stored for 4 weeks at ambient temperature in the glovebox—the same conditions applied during the linking step with the functionalized particles. Poly(butadienyl)lithium is known to cross-link in hydrocarbon solvents at higher temperatures.[34,35] However, although the solution turned yellow during time, in SEC no indication for cross-linking was noticeable even in LS detection, which is sensitive toward traces of higher molecular weight products.

To prove the absence of particle core aggregation during the polymer linking, small-angle X-ray scattering was carried out with the raw product of sample **SiO_2-I-PB1** (Figure 2a) in solution. Because of the similar electron density of the

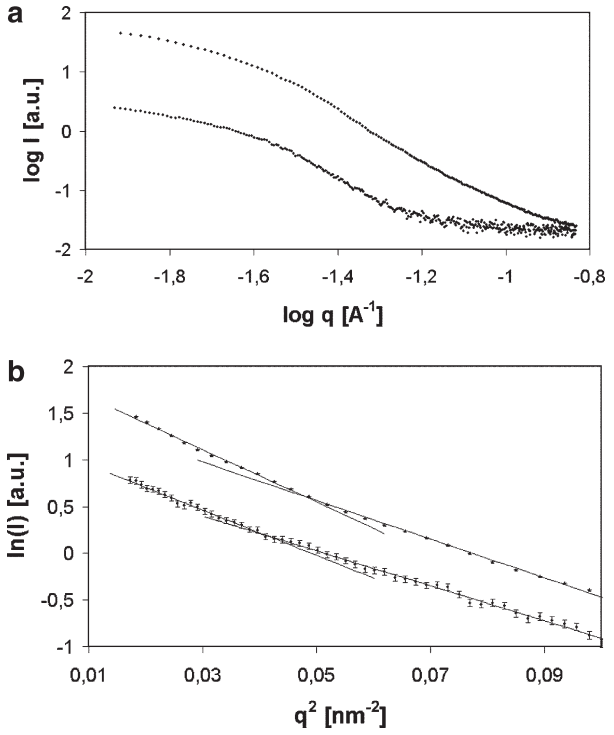

Figure 2. (a) Intensity vs scattering vector q from small-angle X-ray scattering experiments from the raw product of **SiO_2-I-PB1** (lower graph) and the unmodified particles (upper graph) in solution. The Guinier region corresponds to the leveling-off at low scattering vectors. (b) Guinier plot, i.e., $\ln(I)$ vs q^2, of the small-angle X-ray scattering data from the raw product of **SiO_2-I-PB1** (lower graph) and the unmodified particles (upper graph) in solution.

polybutadiene (0.30 $e^-/Å^3$) and the solvent benzene (0.29 $e^-/Å^3$), only the core material (0.60 $e^-/Å^3$) contributes to the scattering signal. Therefore, this method allows gathering information about the size and possible aggregation of the core without influence of the polymer shell. The slight curvature in the Guinier representation of the low q data ($\ln I = \ln I_0 - {}^1/_3 q^2 R_g{}^2$) in Figure 2b is the signature of the modest size distribution in the core dimension. In the equation above, q is the scattering vector defined as $q = (4\pi/\lambda)\sin(\theta/2)$, where λ is the radiation wavelength and θ is the scattering angle (at $q = 0$ the intensity I_0 is the intercept). The range of scattering vectors was restricted to $qR_g \sim 2$, for which the Guinier approximation is valid. The limits of the size distribution can then be estimated from the size determination in both linear extremes. They yield radii of gyration of 7.4 and 8.5 nm, respectively, with uncertainties of ~0.2 nm for the core of **SiO_2-I-PB1**. An average core size can be estimated from the SAXS measurements to $R_g = 7.7$ nm and $\Delta R_g/R_g = (8.5 - 7.7)\text{ nm}/7.7\text{ nm} = 0.1$ can be considered as a lower estimate for the width of the size distribution. The unmodified nanoparticles NBAC-ST show qualitatively the same size distribution pattern (Figure 2a,b). The range of radii of gyration extracted from this measurement in a different setup yields $R_g = 7.9-9.1$ nm, which within the range of the size distribution is identical. This corresponds to hard sphere radii $R \sim 10-12$ nm, knowing that $R_g = ({}^3/_5 R^2)^{1/2}$.[36] The result compares well to the hydrodynamic radius measurement which was described earlier. The consistent results before and after grafting of the polymer chains clearly indicate that during the linking reaction no aggregation of the core material occurs.

In the next step the functionalized nanoparticles were separated from the free polymer by fractionation using

toluene as solvent and methanol as nonsolvent. If this process was carried out in high dilution, almost complete separation was possible in one step. This is shown in Figure 3 for sample **SiO_2-I-PB1**. The lower trace represents the SEC chromatogram of the precipitated functionalized nanoparticles. The upper trace corresponds to the soluble free polymer. The SEC result shows that only minor traces of free polymer remained in the product after one fractionation step.

After the purification by fractionation the functionalized nanoparticles were further characterized by elemental analysis to determine the grafting density. This method is more precise than SEC. Both the carbon and hydrogen content allow determining the amount of polymer in the sample. Because of the higher weight content of carbon, these values were used for determining the polymer content. Together with the molecular weight of the grafted chains and the nanoparticle size the grafting density can be calculated. For **SiO_2-I-PB1**, a grafting density of 0.6 polymer chains/nm^2 was obtained (Table 3). This translates into 760 polymer chains per particle. This is a rather high grafting density compared to other "grafting to" approaches and is in the same range as achievable by "grafting from" techniques.[7] The amount of reacted Si−Cl groups calculated from the carbon content of the polymer functionalized nanoparticles and the polymer molecular weight is 54%. This value is in good agreement with the one calculated before from the analysis of the raw product by SEC and the chlorine content of the chlorosilane functionalized nanoparticles (65%).

Influence of the Polymer Molecular Weight. In the next step the molecular weight of the polybutadiene was increased to 105 000 g mol^{-1} (polymer **PB2-Li** and hybrid particle **SiO_2-I-PB2**). The synthetic procedure was the same as described for **SiO_2-I-PB1**, except that the molar ratio of PB−Li to Si−Cl was increased to 2. Elemental analysis results showed that the grafting density in this case is 0.7 chains/nm^2, which is even somewhat higher than the grafting density of **SiO_2-I-PB1**. This result is unexpected as the polymer molecular weight increases strongly from **PB1** to **PB2** by almost 1 order of magnitude. Because of the positive results obtained so far

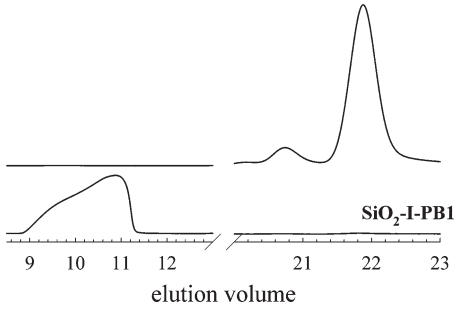

Figure 3. SEC chromatograms of the sample **SiO_2-I-PB1** after fractionation. Upper trace: soluble free polymer; lower trace: precipitated functionalized nanoparticle product.

the polymer molecular weight was again increased to M_n = 589 000 (polymer **PB4-Li** and hybrid particle **SiO_2-I-PB4**). The molar ratio of PB−Li to Si−Cl was raised to 2.3 to compensate for possible impurities in the reaction mixture as the reaction had to be carried out in higher dilutions with increasing polymer molecular weight. Because of the large size of the resulting particles, monitoring the reaction by SEC was not possible, and fractionation of the particles became more difficult (see Experimental Section). Elemental analysis of the pure particles revealed a grafting density of 0.2 chains/nm^2, which corresponds to ~218 chains per particle. Because of the high carbon content of the sample (85.4%) compared to the one of the pure polymer (88.8%), the determination of the grafting density becomes rather difficult by elemental analysis. To confirm these results, the molecular weight of the hybrid particle was additionally measured by static light scattering. The molecular weight of **SiO_2-I-PB4** results in 167 × 10^6 g/mol. The number of chains per particle calculated from this result is 275, and the chain density is 0.2 chains/nm^2. Premature termination of the living headgroups could be excluded for **SiO_2-I-PB4**. After addition of dry THF the solution turned yellow, which indicates the presence of still active PB−Li. This experiment shows that even for extremely high polymer molecular weights visible grafting still is possible; however, the grafting density decreases due to sterical restrictions. The particles showed a large increase in size. The hydrodynamic radius was determined to be R_h = 186 nm.

R_h of **SiO_2-I-PB1** in heptane was measured to be 34 nm. The comparison with the particles before grafting of the polymer chain (R_h = 13 nm for **SiO_2-Cl-I**) yields a thickness of the polymer shell of 21 nm. The R_h of the free polymer chain was calculated to be 3.6 nm for **PB1**. This result can only be explained provided that already for the smallest molecular weight the attached polymer chains are stretched. This scenario repeats for samples **SiO_2-I-PB2** and **SiO_2-I-PB4**. Furthermore, the DLS results show for all samples the absence of aggregation of the formed hybrid nanoparticles.

Influence of the Si−Cl Grafting Density at Constant Molecular Weight. In order to investigate the influence of the Si−Cl density on the polymer functionalization, the nanoparticles **SiO_2-Cl-II** and **SiO_2-Cl-III** were synthesized. Compared to the chlorosilane-functionalized nanoparticles **SiO_2-Cl-I** used so far, the density of Si−Cl groups is lowered for **SiO_2-Cl-II** and is increased for **SiO_2-Cl-III** (Table 1). The reaction of **SiO_2-Cl-III** with **PB3-Li** proceeded under the same PB−Li to Si−Cl ratio as the functionalization of **SiO_2-Cl-I**. Although the neat **SiO_2-Cl-III** particles could only partially be redispersed after Si−Cl functionalization, they are almost fully solubilized with ongoing reaction with the living polymer. Only very small amounts of insoluble residues were left at the end of the linking reaction. This indicates a reversible aggregation during the functionalization with $SiCl_4$ rather than cross-linking via covalent bonds. After fractionation, a grafting density of

Table 3. Reaction Conditions and Characterization of the Polymer-Functionalized Nanoparticles

hybrid nanoparticle	particle	polymer	molar ratio of PB−Li/SiCl	M_n of polymer (g/mol)	grafting density (chains/nm^2)	R_h (nm)
SiO_2-I-PB1	**SiO_2-Cl-I**	**PB1**	1.5	15 300	0.6	34
SiO_2-I-PB2	**SiO_2-Cl-I**	**PB2**	2	105 000	0.7	88
SiO_2-II-PB3	**SiO_2-Cl-II**	**PB3**	6.6	13 000	0.5	28
SiO_2-III-PB3	**SiO_2-Cl-III**	**PB3**	1.5	13 000	1.0	35
SiO_2-I-PB4	**SiO_2-Cl-I**	**PB4**	2.3	589 400	0.2	186
SiO_2-I-PS1	**SiO_2-Cl-I**	**PS1**	2	10 100	0.5	18
SiO_2-I-PS-PB1	**SiO_2-Cl-I**	**PS-PB1**	2	10 100	0.7	19

Table 4. Reaction of SiO_2-Cl-I with Different Amounts of PB−Li

hybrid nanoparticle	particle	polymer	molar ratio of PB−Li/SiCl	fraction of grafted polymer (%)	grafting density (chains/nm^2)	fraction of reacted Si−Cl (%)
SiO_2-I-PB3a	**SiO_2-Cl-I**	**PB3**	0.5	19	0.1	10
SiO_2-I-PB3b	**SiO_2-Cl-I**	**PB3**	1	28	0.3	28
SiO_2-I-PB1	**SiO_2-Cl-I**	**PB1**	1.5	43	0.7	65
SiO_2-I-PB3c	**SiO_2-Cl-I**	**PB3**	3.2	30	1.1	97

1.0 polymer chain/nm^2 was determined by elemental analysis for the product **SiO_2-III-PB3**. This value is visibly higher than the 0.6 polymer chains/nm^2 for **SiO_2-I-PB1**. The difference can originate from the higher Si−Cl functionality of the nanoparticle starting material, which is 5.06 Si−Cl/nm^2 for **SiO_2-Cl-III** and 1.12 Si−Cl/nm^2 for **SiO_2-Cl-I**. However, the remaining Si−OH groups on the nanoparticle surface have also to be considered. Therefore, the ratio of original PBLi to Si−OH needs to be taken into account. This is drastically higher for **SiO_2-III-PB3** if one considers the density of remaining Si−OH groups being approximately equal in **SiO_2-Cl-I** and **SiO_2-Cl-III**. This can influence the polymer functionalization reaction, too, especially if one takes into account that in experiment **SiO_2-I-PB1** all added polymer was terminated during the reaction with the nanoparticles.

SiO_2-Cl-II, with only 0.36 Si−Cl/nm^2 is totally insoluble and undispersible in benzene in contrast to the other chlorosilane functionalized nanoparticles. Nevertheless, the reaction with **PB3-Li** was investigated. During the reaction, a slow solvation of the nanoparticles within several hours to a totally clear solution could be noticed. This result indicates that no irreversible cross-linking via covalent bonds occurred during chlorosilane functionalization. The resulting hybrid particles **SiO_2-II-PB3** showed a similar behavior to **SiO_2-I-PB1** and **SiO_2-III-PB3**. After fractionation, the grafting density was determined to be 0.5 chains/nm^2. This result is inconsistent with the degree of chlorosilane functionalization of only 0.36 Si−Cl groups/nm^2. Because of analysis by SEC and the fractionation step, a contamination with reversibly adsorbed polymer chains on the particles can be excluded. Potential side reactions of PB−Li with the silica surface are currently investigated in detail to explain the higher grafting density obtained with **SiO_2-Cl-II**.[37,38] Irrespectively to the unusually high grafting density, **SiO_2-II-PB3** shows a distinctively lower grafting density compared to **SiO_2-III-PB3**. This is mirrored in the hydrodynamic radius, which is remarkably lower for **SiO_2-II-PB3** compared to **SiO_2-III-PB3** (see Table 3).

In another series of experiments the PB−Li concentration was varied at fixed Si−Cl grafting density. Table 4 summarizes the results from the reactions with **SiO_2-Cl-I**. The amounts of polymer linked on the particles were determined by SEC examination of the raw products as described before. In these cases the products were not fractionated so that elemental analysis was not possible.

The grafting density clearly increases with increasing amounts of PB−Li and reaches nearly 100% functionalization of the available Si−Cl binding sites at a ratio of PB−Li to Si−Cl of 3.2. This result shows that both methods, increasing the Si−Cl density as well as increasing the PB−Li to Si−Cl ratio, help to obtain high polymer grafting densities. To determine whether still living polymer remained, butadiene was added to a sample of each reaction mixture after the linking reaction had stopped according to the SEC analysis. In the samples up to 1.5 equiv of PB−Li per Si−Cl no molecular weight increase of the free polymer was detected. The scenario is different for the highest PB−Li to Si−Cl ratio in sample **SiO_2-I-PB3c**. Upon butadiene addition SEC analysis revealed an additional signal at higher molecular weight than **PB3**. From the amounts of PB−Li and added butadiene as well as the molecular weight increase of the additionally formed polymer, the amount of still active headgroups was calculated to be 20% of the originally added PB−Li.

Influence of the Grafted Polymer. Besides the grafting of PB−Li, polystyryllithium (PS−Li) was reacted with the functionalized silica particles (Scheme 3). The polystyrene-grafted particles are directly comparable to those obtained by the "grafting from" techniques using controlled radical polymerization and are of interest due to the wide use of polystyrene in various applications. The reaction of **SiO_2-Cl-I** with **PS1-Li** was found to proceed similar to the grafting of polybutadiene. Even the fractionation step to purify the resulting hybrid nanoparticles **SiO_2-I-PS1** was performed under the same conditions as worked out for the purification of the polybutadiene counterparts. According to the elemental analysis, the grafting density of polystyrene chains was determined to be 0.5 chains/nm^2 for **SiO_2-I-PS1** (Table 3). As the reaction mixture was colored orange all the time, living polymer was present until termination. This indicates that for PS 0.5 chains/nm^2 is the upper limit of the grafting density obtainable with our "grafting to" technique. Although still being high compared to other "grafting from" approaches reported in the literature, the PS functionalization leads to a lower grafting density than achievable with polybutadiene. In the analogue PB experiment **SiO_2-PS8** living PB-Li was present until termination and the final grafting density was 1.0 chains/nm^2. This result is understandable if the higher sterical demand of the PS-Li headgroup is considered (see Scheme 3). It is in accordance with the results for the synthesis of star polymers. For example, PS-Li reacts only partially with $SiCl_4$ due to sterical restrictions at the star center.[22] For the synthesis of multiarmed polystyrene star polymers, the polystyrene has therefore to be end-capped with a few monomer units of butadiene before reacting with the chlorosilane.[24] Therefore, we applied the same concept for the functionalization of the nanoparticles (see Scheme 3). End-capping of **PS1-Li** with ~4 units of butadiene led to the living anionic polymer **PS-PB1-Li**. The reaction of **PS-PB1** with **SiO_2-Cl-I** and subsequent fractionation yielded hybrid nanoparticles with a grafting density of 0.7 chains/nm^2 (Table 3). This is in agreement with the results obtained by using PB−Li and is also comparable with the grafting densities accessible via "grafting from" approaches.

Discussion

Termination Process. In all the reactions of the living anionic polymer with the functionalized particles, significant amounts of free and terminated polymer were formed as a side product. It is likely that residual Si−OH groups at the nanoparticle surface cause this process (Scheme 4). According to our analysis of the Si−Cl functionalized particles, 33% of originally 5.5 Si−OH groups stay unmodified. This value translates into 1.82 remaining Si−OH/nm^2. IR spectroscopy of **SiO_2-Cl-I** in dry chloroform in a CaF_2 cuvette filled under argon atmosphere qualitatively supports this assumption. The measurement showed an absorption band in the range

Scheme 4. Possible Termination Reaction of the Anionic Headgroups

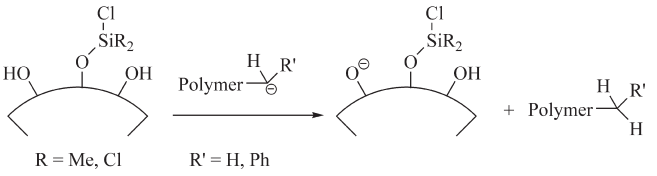

Table 5. Amounts of Polymer Reacted with Si−Cl, Terminated with Si−OH, or Remaining Unreacted[a]

	PB−Li/nm^2			
hybrid nanoparticle	overall	remaining PB−Li[b]	terminated with Si−OH[c]	reacted with Si−Cl[b]
SiO_2-I-PB3a	0.56	0	0.45	0.11
SiO_2-I-PB3b	1.12	0	0.81	0.31
SiO_2-I-PB1	1.68	0	1.01	0.67
SiO_2-I-PB3c	3.58	0.72	1.77	1.09

[a] All values are normalized to the nanoparticle surface. In all cases nanoparticles **SiO_2-Cl-I** were used, which contain 1.12 Si−Cl and 1.82 Si−OH per nm^2 of surface. [b] Obtained from the SEC analysis of the samples after addition of extra monomer. [c] Calculated from the amounts of PB−Li reacted with Si−Cl and the amounts of remaining PB.

from 3600 to 3700 cm^{-1} which can be attributed to the O−H vibrational band.[29−31]

To investigate the competitive termination and linking reactions, **SiO_2-Cl-I** was treated with different amounts of **PB1-Li** or **PB3-Li** (see Table 4). Subsequent butadiene addition allowed distinguishing between terminated and still active living polymer. For the PB−Li to Si−Cl ratios up to 1.5:1 in samples **SiO_2-I-PB3a**, **SiO_2-I-PB3b**, and **SiO_2-I-PB1** no remaining living polymer was found. This result is in agreement with the finding from experiment **SiO_2-I-PB2** where also no living polymer remained for a PB−Li to Si−Cl ratio of 2. The corresponding functionalized nanoparticles **SiO_2-Cl-I** contain 1.12 Si−Cl groups and 1.82 Si−OH groups per nm^2. On the other hand, the original content of living polymer in the reaction mixture of sample **SiO_2-I-PB2** was 2.24 PB−Li per nm^2 of the silica surface. Therefore, full termination is not unexpected. The scenario first changes with sample **SiO_2-I-PB3c**. Here the amount of PB−Li exceeds the quantities of Si−Cl and Si−OH. Consequently, in this sample remaining living polymer was found after the linking reaction. Table 5 quantifies for the samples listed in Table 4 the fractions of polymer having reacted with Si−Cl and Si−OH or being still living after the end of the linking reaction. The quantities of terminated polymer were calculated as diffence between the original polymer amounts and the amounts of grafted and remaining living polymer. For sample **SiO_2-I-PB3c** the terminated amount is almost identical with the calculated Si−OH content. This value was obtained from the analysis of the Si−Cl functionalized particles estimating the original Si−OH density to be 5.5 per nm^2. It seems that this estimation is quite accurate because of the agreement between terminated polymer and Si−OH content.

Another interesting aspect arises from the comparison of the polymer fractions which were linked with Si−Cl or terminated with Si−OH. From the comparison of the values it can be concluded that the termination reaction with Si−OH is preferred against the linking reaction with Si−Cl. Therefore, an excess of PB−Li is required to obtain higher grafting densities.

To reduce the amount of terminated polymer, experiments were performed by reacting **SiO_2-Cl-I** with *sec*-butyllithium prior to the functionalization with PB−Li. This strategy was chosen as a consequence of the faster termination reaction compared to the linking event. Therefore, *sec*-butyllithium should also preferably react with Si−OH rather than being linked to the nanoparticles via reaction with the Si−Cl groups. Unfortunately, the addition of 1 or 2 equiv of *sec*-butyllithium relative to Si−Cl to **SiO_2-Cl-I** did not reduce the amount of terminated PB−Li.

Grafting Density. In this work two methods were used to measure the polymer grafting densities. The first one is based on the carbon content determination by elemental analysis of the fractionated hybrid nanoparticles. Together with the polymer molecular weight and the knowledge of the nanoparticle size the grafting density can be calculated. The second method is based on SEC analysis which allows quantifying the free polymer content of the raw product after functionalization. From this result the quantity of grafted polymer can be calculated and with the nanoparticle size the grafting density is obtained. For sample **SiO_2-I-PB1** both methods were applied (see Tables 3 and 4). Both values are in good agreement. This underlines that the experimentally much easier SEC based method is an accurate measure for determining the grafting density.

Using the "grafting to" approach described in this work, the grafting density is generally determined by two factors. This is first the density of Si−Cl groups at the nanoparticle surface in combination with the PB−Li excess. The treatment with chlorosilanes produces a densely functionalized surface. This becomes clear in the following estimation. The molecular volume of Me_2SiCl_2 is about 0.20 nm^3. This value simply can be calculated from its density and molecular weight. If for simplification the shape of the molecule is assumed to be spherical, one expects that each molecule covers a surface of 0.40 nm^2, or in other words, the surface can contain up to 2.5 silane molecules per nm^2. On the basis of our analysis the Me_2SiCl_2-treated surface contains about 2.9 silane units per nm^2, namely 1.12 O−Si Me_2Cl and 0.72 O−Si Me_2 units as well as 1.1 O−Si Me_3 resulting from the hydrophobical modification. It is clear that the different silane units have different sizes, and our estimation did not consider the three-dimensional topology of the silica surface or the limited spatial requirements of the surface bound units due to lesser thermal fluctuations. Nevertheless, the comparison shows that the surface functionalization obtained with the chlorosilanes is extremely dense.

As the linking process is in competition with termination always a polymer excess is required. If this is taken into account, full conversion of the Me_2SiCl linking sites can be achieved for nanoparticles being functionalized with Me_2SiCl_2 (experiment **SiO_2-I-PB3c**, Table 4). If Me_2SiCl_2 is replaced by $SiCl_4$, the Si−Cl density is increased significantly. This is valid if the density is expressed in Si−Cl units or in chlorosilane-containing groups. The reason for this is that in case of $SiCl_4$ after double or even triple reaction of the chlorosilane with the surface still Si−Cl functionalities remain. On the contrary, Me_2SiCl_2 looses its Si−Cl functionality already if double reaction occurs. Regardless, the higher Si−Cl density the $SiCl_4$-functionalized nanoparticles do not generate a higher polymer density. This becomes apparent by comparing samples **SiO_2-I-PB3c**, functionalized with Me_2SiCl_2, and **SiO_2-III-PB3**, functionalized with $SiCl_4$. Both samples have similar polymer grafting densities, and in both experiments there still was living polymer present after the reactions stopped. Therefore, insufficient living polymer because of termination effects did not play a role. It seems that instead the limiting factor is the high polymer density at the surface, and about 1 chain/nm^2 appears to be the upper limit.

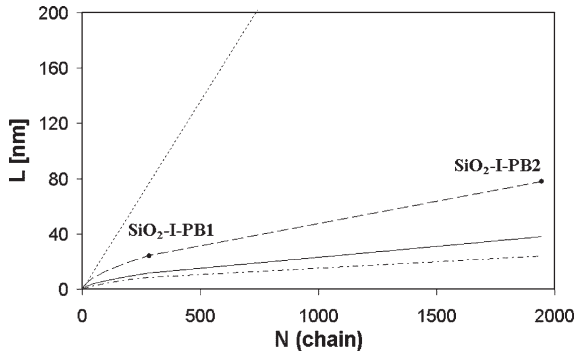

Figure 4. Estimations of the shell thickness L as a function of the polymerization degree of the attached chains N. For a grafting density of 0.65 chains/nm^2 different models are compared with measured values of samples having approximately the same grafting density: compact polymer shell (dash-dotted curve), estimation based on R of the free polymer chain (solid curve), Daoud−Cotton model (dashed curve), and Alexander model (dotted curve).

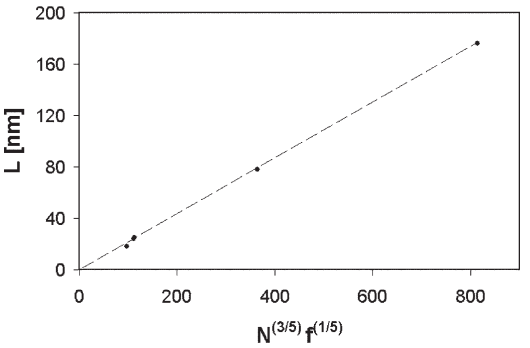

Figure 5. Shell thickness L vs $N^{0.6}f^{1/5}$ for all hybrid particles with a polybutadiene shell (samples **SiO_2-I-PB1**, **SiO_2-I-PB2**, **SiO_2-II-PB3**, **SiO_2-III-PB3**, and **SiO_2-I-PB4**).

The second factor comprises the local sterical demand of the polymer headgroups as well as the overall stretching of the polymer chain, especially at higher polymer densities. Therefore, it is understandable that the "grafting to" approaches reported in the literature are limited to low grafting densities.

The new method presented in this work allows synthesizing hybrid materials of much higher chain densities and having interchain distances much smaller than R_g. As a consequence, the chains must be stretched. This already gets clear by comparing the R_h values of the polymer modified particles (Table 3) with the ones for the corresponding free polymers (Table 2). The accessibility of high grafting densities are understandable if one considers a polymer chain as a dynamic object which a fraction of the time is considerably more stretched than in the thermodynamic equilibrium state. Once the highly reactive chain end comes close to a chlorosilane linking group on the surface, the covalent bond is irreversibly formed.

In order to get an idea of the shell thickness L as a function of the PB molecular weight, different models were compared. The results are shown in Figure 4. For reasons of comparability the grafting density was fixed to 0.65 chains/nm^2. The core radius was $R_{core} = 10$ nm. In the lowest estimation the shell thickness was assumed containing no solvent and the polymer shell having the same density as the bulk polymer (dash-dotted line). In a good solvent the shell thickness must increase due to the swelling of the polymer chains. Therefore, more realistic results for the lower limit of the shell thickness are obtained if the size of the free polymer in a good solvent is used. To keep the results consistent with the other estimations, the hard sphere radius R was used as a measure for the size of the swollen polymer coils. The use of R_g underestimates the polymer size. In Figure 4 the hard sphere diameter D is plotted (solid line). D was calculated following the equation $D = 2R = 2(5/3)^{1/2}R_g$. R_g was calculated according to the equation $R_g = 1.29 \times 10^{-2}M^{0.609}$.[33] The upper limit for the shell thickness can be calculated by the Alexander model for polymer chains on a flat surface (dotted line).[39] In this model, a chain stretching factor as a function of the grafting density is included. The shell thickness is given by $L = Nl\sigma_k^{1/3}$, with l being the length of one monomer unit and N being the polymerization degree of the attached chains. σ_k is a measure for the grafting density with $\sigma_k = Pl^2/(4\pi R_{core}^2)$. P is the number of polymer chains. This model drastically overestimates the shell thickness since a flat surface offers constant space with increasing distance to the particle surface. For a spherical surface as in our case the space increases quadratically with increasing R. The measured shell thicknesses are situated between the upper and lower limits. Figure 4 contains the results for **SiO_2-I-PB1** (grafting density 0.6 chains/nm^2) and **SiO_2-I-PB2** (grafting density 0.7 chains/nm^2). The shell thicknesses were obtained from the R_h values of the hybrid particles according to the equation $L = R_h - R_{core}$.

To get a realistic description of the shell thickness with increasing molecular weight, the model proposed by Daoud and Cotton for star polymers is useful. For long polymer arms, the relationship between L and N as well as the number of grafted chains f is given by $L = \alpha N^{0.6}f^{1/5}$.[40] Figure 5 demonstrates how well this assumption describes the measured shell thicknesses. The plot contains the measured shell thicknesses of the PB samples **SiO_2-I-PB1**, **SiO_2-I-PB2**, **SiO_2-II-PB3**, **SiO_2-III-PB3**, and **SiO_2-I-PB4**. The samples cover a polymerization degree range between 240 (**SiO_2-II-PB3** and **SiO_2-III-PB3**) and 10 900 (**SiO_2-I-PB4**) as well as a grafting density range between 0.2 chains/nm^2 (**SiO_2-I-PB4**) and 1.0 chains/nm^2 (**SiO_2-III-PB3**). The scaling coefficient R was obtained from fitting the data points ($R^2 = 0.9996$). A value of $\alpha = 0.217$ was obtained. The dashed curve in Figure 4 was obtained with this scaling coefficient.

According to the findings from above, the thickness of the polymer shell in a good solvent scales with $N^{0.6}$. For free polymer chains under the same conditions R_g or R_h scale with $N^{0.6}$, too. Therefore, the stretching of polymer chains attached on a spherical surface is independent of their length. The stretching factor S of the attached chains can be estimated to be $S = L/D$. According to this formula, the polymers are not strongly stretched. S reaches values between 2 and 2.5 for the samples having the highest grafting densities. With this knowledge it is understandable that up to a polymer molecular weight of 105 000 g/mol a high grafting density could be obtained (sample **SiO_2-I-PB2**). The reason for the drop in grafting density for the highest molecular weight of 589 000 g/mol (sample **SiO_2-I-PB4**) might be a kinetic effect because of the increasing viscosity of the reaction medium.

The high chain density accessible with our synthetic approach additionally can be demonstrated by comparison with the chain density in the bulk. Under the assumption that all chains are oriented in parallel, the maximum density is 5 chains per nm^2 in the case of PB. This value simply can be calculated from the length and volume of a monomer unit. The latter value is accessible with the knowledge the polymer bulk density and the monomer mass. Synthetically, the maximum density is 1 chain per nm^2 at the nanoparticle surface. If one considers that even at the surface the chains

are not oriented in parallel, it is obvious that the achievable chain density is extremely high. For PS the maximum bulk density is 1.6 parallel chains per nm^2. Without end-capping it was possible to graft 0.5 chains per nm^2 of nanoparticle surface. After end-capping with 4 units of butadiene this value increased to 0.7 chains. This comparison shows that first for PS the grafting density is even higher if the bulkiness of the chains is considered and second end-capping with a less bulky monomer is useful to overcome spatial restrictions. The maximum chain density which was obtained using the grafting from approach via ATRP on exactly the same nanoparticle material as used in this work was 0.9 chains/nm^2 for PS.[7] It is obvious that this value is near to the upper limit due to the spatial restrictions.

The comparison of our synthetic approach with the synthesis of star polymers using chlorosilane dendrimers is instructive, too. For 16-, 32-, and 64-arm star polymers synthesized with dendritic linking agents the Si−Cl groups react almost quantitatively with the living polymers.[27] The grafting density at the hypothetical dendrimer surface can be calculated assuming the dendritic core to be spherical and the inner dendrimer bonds having exclusively fully stretched all-trans configurations. The latter assumption seems quite realistic due to the osmotic pressure caused by the high polymer density near the core. On this basis the chain density increases from 2.0 arms per nm^2 for a 16-arm star to 2.6 arms per nm^2 for a 64-arm star. The core radius in case of the 64 arm star is 1.3 nm. Because of the stronger curvature compared to the nanoparticles, there is more space in the outer parts of the star corona and chains are less stretched. Additionally, the dendrimer surface offers a more open reaction space than the compact nanoparticle surface. Nevertheless, this comparison underlines that it is not unusual obtaining relatively high grafting densities using the "grafting to" approach.

Conclusion

In the past mainly controlled radical techniques in combination with the "grafting from" method were used to graft polymers onto nanoparticles or other solid surfaces. This work demonstrates that the "grafting to" approach represents a powerful alternative by reacting living anionically produced polymers with chlorosilane-modified surfaces. Both the functionalization of silica nanoparticles with multifunctional chlorosilane agents and the subsequent reaction with living polymer can be effected without irreversible particle aggregation. As the polymer linking event is accompanied by termination reactions, the polymer cannot be linked to the nanoparticles quantitatively. The new anionic-based method offers the possibility for much higher grafting densities than reported in the past for other "grafting to" approaches. The now obtained grafting densities are similar to the ones reported for controlled radical "grafting from" techniques.

Generally, the controlled radical techniques are advantageous for synthesizing hybrid materials being functionalized with polymers of lower molecular weights. In this case the hybrid material can be produced without or with only small quantities of free polymer as side-product and polymer molecular weight distributions are low. The scenario changes for hybrid materials containing high molecular weight polymers. Here, contamination with free polymer comes into play in case of radically synthesized polymers due to additional thermal initiation. Additionally, molecular weight distributions broaden, which is not the case for anionically produced polymers. Furthermore, the anionic-based method allows access to hybrid materials containing polymers which cannot be synthesized in a controlled way by radical methods like the polydienes. Another advantage of the implementation of anionic polymerization into the hybrid material synthesis is the accessibility of well-defined block copolymers. Even advanced controlled radical techniques like ARGET ATRP are of limited use in this case.[15] Our current work now focuses on investigating the details of the linking process as well as the nature of the termination process in order to minimize the amount of terminated polymer.

Acknowledgment. This work was funded by the European Union under the FP7-NMP-2007 program, Nanomodel Grant Agreement SL-208-211778.

Supporting Information Available: Detailed synthesis procedure for **SiO_2-I-PB1**. This material is available free of charge via the Internet at http://pubs.acs.org.

References and Notes

(1) Gravano, S. M.; Patten, T. E. In *Macromolecular Engineering: Precise Synthesis, Materials Properties, Applications*; Matyjaszewski, K., Gnanou, Y., Leibler, L., Eds.; Wiley-VCH: Weinheim, 2007; Vol. *2*, Chapter 12, pp 1179−1207.
(2) Gravano, S. M.; Dumas, R.; Liu, K.; Patten, T. E. *J. Polym. Sci., Part A: Polym. Chem.* **2005**, *43*, 3675–3688.
(3) Saleh, N.; Sarbu, T.; Sirk, K.; Lowry, G. V.; Matyjaszewski, K.; Tilton, R. D. *Langmuir* **2005**, *21*, 9873–9878.
(4) Bombalski, L.; Dong, H.; Listak, J.; Matyjaszewski, K.; Bockstaller, M. R. *Adv. Mater.* **2007**, *19*, 4486–4490.
(5) Radhakrishnan, B.; Ranjan, R.; Brittain, W. J. *Soft Matter* **2006**, *2*, 386–396.
(6) von Werne, T.; Patten, T. E. *J. Am. Chem. Soc.* **1999**, *121*, 7409–7410.
(7) Pyun, J.; Jia, S.; Kowalewski, T.; Patterson, G. D.; Matyjaszewski, K. *Macromolecules* **2003**, *36*, 5094–5104.
(8) Carrot, G.; Harrak, A. E.; Oberdisse, J.; Jestin, J.; Boué, F. *Soft Matter* **2006**, *2*, 1043–1047.
(9) Dong, H.; Zhu, M.; Yoon, J. A.; Gao, H.; Jin, R.; Matyjaszewski, K. *J. Am. Chem. Soc.* **2008**, *130*, 12852–12853.
(10) Savin, D. A.; Pyun, J.; Patterson, G. D.; Kowalewski, T.; Matyjaszewski, K. *J. Polym. Sci., Part B: Polym. Phys.* **2002**, *40*, 2667–2676.
(11) Tsujii, Y.; Ejaz, M.; Sato, K.; Goto, A.; Fukuda, T. *Macromolecules* **2001**, *34*, 8872–8878.
(12) Ando, T.; Kamigaito, M.; Sawamoto, M. *Macromolecules* **1998**, *31*, 6708–6711.
(13) Coessens, V.; Matyjaszewski, K. *Macromol. Rapid Commun.* **1999**, *20*, 66–70.
(14) Matyjaszewski, K.; Davis, K.; Patten, T. E.; Wei, M. *Tetrahedron* **1997**, *53*, 15321–15329.
(15) Jakubowski, W.; Kirci-Denizli, B.; Gil, R. R.; Matyjaszewski, K. *Macromol. Chem. Phys.* **2008**, *209*, 32–39.
(16) Advincula, R.; Zhou, Q.; Park, M.; Wang, S.; Mays, J.; Sakellariou, G.; Pispas, S.; Hadjichristidis, N. *Langmuir* **2002**, *18*, 8672–8684.
(17) Cosgrove, T.; Heath, T. G.; Ryan, K. *Langmuir* **1994**, *10*, 3500–3506.
(18) Duchet, J.; Chapel, J.-P.; Chabert, B.; Spitz, R.; Gérard, J.-F. *J. Appl. Polym. Sci.* **1997**, *65*, 2481–2492.
(19) Derouet, D.; Forgeard, S.; Brosse, J.-C. *Macromol. Chem. Phys.* **1999**, *200*, 10–24.
(20) Viswanathan, K.; Long, T. E.; Ward, T. C. *J. Polym. Sci., Part A: Polym. Chem.* **2005**, *43*, 3655–3666.
(21) Gilman, H.; Cartledge, F. K. *J. Organomet. Chem.* **1964**, *2*, 447–454.
(22) Roovers, J. E. L.; Bywater, S. *Macromolecules* **1972**, *5*, 384–388.
(23) Roovers, J. E. L.; Bywater, S. *Macromolecules* **1974**, *7*, 443–449.
(24) Roovers, J.; Hadjichristidis, N.; Fetters, L. J. *Macromolecules* **1983**, *16*, 214–220.
(25) Hadjichristidis, N.; Roovers, J. E. L. *J. Polym. Sci.* **1974**, *12*, 2521–2533.
(26) Roovers, J.; Toporowski, P.; Martin, J. *Macromolecules* **1989**, *22*, 1897–1903.
(27) Allgaier, J.; Martin, K.; Räder, H. J.; Müllen, K. *Macromolecules* **1999**, *32*, 3190–3194.
(28) Suzuki, T.; Hitoshi, E.; Shibayama, M. *Langmuir* **2008**, *24*, 4537–4543.

(29) Hair, M. L. *Infrared Spectroscopy in Surface Chemistry*; Marcel Dekker: New York, 1967.
(30) Hertl, W.; Hair, M. L. *J. Phys. Chem.* **1971**, *75*, 2181–2185.
(31) Snyder, L. R.; Ward, J. W. *J. Phys. Chem.* **1966**, *70*, 3941–3952.
(32) Stenkamp, V. S.; Berg, J. C. *Langmuir* **1997**, *13*, 3827–3832.
(33) Fetters, L. J.; Hadjichristidis, N.; Lindner, J. S.; Mays, J. W. *J. Phys. Chem. Ref. Data* **1994**, *23*, 619–640.
(34) Morton, M.; Fetters, L. J. *J. Polym. Sci., Part A: Polym. Chem.* **1964**, *2*, 3311–3326.
(35) Viola, G. T.; Bortolotti, M.; Zazzetta, A. *J. Polym. Sci., Part A: Polym. Chem.* **1996**, *34*, 13–24.
(36) Guinier, A.; Fournet, G. In *Small Angle Scattering of X-rays*: J. Wiley & Sons: New York, 1955.
(37) Lim, J. E.; Shim, C. B.; Kim, J. M.; Lee, B. Y.; Yie, J. E. *Angew. Chem., Int. Ed.* **2004**, *43*, 3839–3842.
(38) Kecht, J.; Bein, T. *Langmuir* **2008**, *24*, 14209–14214.
(39) Alexander, S. *J. Phys.* (*Paris*) **1977**, *38*, 983–987.
(40) Daoud, M.; Cotton, J. P. *J. Phys.* (*Paris*) **1982**, *43*, 531–538.